OPTIMISING HIGH-EFFICIENCY RUDDERS FOR TRANSPORT AIRCRAFT FUEL BURN REDUCTION

M. Laban, M.H. Smaili, D.R. van der Heul, P. Arendsen, B.A.T. Noordman
National Aerospace Laboratory NLR, Amsterdam, the Netherlands.

Keywords: *double-hinged rudder, vertical tail plane*

Abstract

The wetted surface of the vertical tail plane, or shortly VTP, is a significant contributor to the drag, and hence fuel burn, of transport aircraft. For a configuration with under-wing mounted engines, the VTP sizing is typically based on a one engine-out scenario at minimum control speed. In this condition, the VTP with fully deflected rudder must produce a side force to counteract the yawing moment arising from the asymmetric engine thrust setting. Applying a more effective rudder allows the VTP size to reduce, hence the aircraft cruise drag to reduce. A higher effectiveness of the rudder can be obtained by segmenting the rudder surface into two mechanically linked segments. This paper explores optimal settings for the two rudder segments. An application is presented for a medium-range generic transport aircraft configuration. It is concluded that a double-hinged rudder, comprising a relatively small second rudder segment, offers 0.5% cruise drag reduction potential at almost identical VTP mass. The rudder actuation servo forces increase. Aircraft lateral/directional stability reduces and this may require re-tuning of the yaw damper gains.

1 Introduction

Increasing oil prices and a growing public concern on the effect of aviation on global climate change, re-enforces the market for low fuel burn aircraft. In the past decades, new engine technology and the breakthrough of new aircraft materials (composites) were successful enablers in this respect. Also the aerodynamics discipline contributes. For transport aircraft, the viscous drag component dominates and is responsible for about 70% of the total drag in cruise. The most straightforward means for viscous drag reduction is to reduce the aircraft wetted surface. The tail planes do provide opportunities for wetted surface reduction which have not yet been fully exploited on transport aircraft in service today.

The current paper focuses on the vertical tail plane (VTP). An analysis has also been made for the horizontal tail plane (HTP). The VTP results, however, seem to be more promising.

The VTP provides aircraft lateral/directional stability and control. With the advent of full authority digital control, which can provide yaw rate feedback even when flown in backup mode, there is an opportunity to relax the requirements on the inherent (lateral/directional) stability of the basic airframe. Hence, this provides an opportunity to reduce the VTP size. However, the requirement on the maximum side force the VTP with fully deflected rudder can deliver to counter yawing moments that may occur in extreme flight conditions will not change. E.g. one engine-out & cross-wind landing requirements are typical conditions driving the VTP size. This calls for a higher effectiveness of the rudder to compensate for the smaller VTP size.

Increasing the effectiveness of the rudder at full deflection can be done by applying an optimal cambering of the devices downstream of the VTP structural box. Advances in morphing materials may one day deliver the technology to do so

in a truly optimal sense. Short time horizon practical solutions, however, make use of multiple mechanically linked rudder segments. Double-hinged rudders are found on several transport aircraft in service today (e.g. DC-10, B-777, ERJ-145). All these arrangements seem to have chosen a common concept in which the second rudder segment hinge line is positioned mid-way the first rudder segment hinge line position and the trailing edge.

The paper will quantify the potential of an optimised double-hinged device relative to the classical single-hinged solution for the VTP. Various disciplines will be addressed. The aerodynamics discipline will explore optimal settings for the second rudder segment hinge line position as well as the ratio of second rudder segment versus first rudder segment deflection angles. The systems discipline will investigate rudder drive solutions and quantifies the consequences on servo force requirements. The flight mechanics discipline will investigate the impact on the aircraft lateral-directional stability and control. The loads and structural mechanics discipline will evaluate the impact on the VTP overall mass.

The paper is illustrated with results obtained for an application to a medium-range 180 seat generic transport aircraft configuration.

2 VTP Geometry

Two different VTP geometries, with increasing complexity, are used in the study. The first step, *aerodynamic optimisation*, requires short problem turn around times for which an isolated-VTP mounted on a symmetry plane offers a suitable representation. The second step, *aerodynamic assessment*, requires a more complete geometry in which the VTP is mounted on a generic transport aircraft fuselage & HTP configuration.

The rudder contours are cut from the VTP definition section downstream of the hinge line station (defined in terms of a fixed ratio of chord x_h/c) and are complemented with tapered cylindrical nose sections. The rudders are rotated over the hinge line vector to the required deflection angle. The remaining VTP contours upstream the hinge line position are "shortened" to allow the rudders to rotate to their maximum deflection angles (positive & negative). This results in 0.5% chord length *rudder gaps* which are included in the geometry as small backward facing steps.

The VTP planform parameters are: area $21.5m^2$, aspect ratio 1.62, taper ratio 0.34, quarter chord sweep angle 35^o. The VTP cross-sections are based on the 11% thickness-to-chord ratio NACA64A011 airfoil. The following discrete choices for the rudder parameters are made:

- fixed first rudder segment hinge line position relative to chord, $x_{h1}/c = 0.70$,
- variable second rudder segment hinge line position relative to chord, $x_{h2}/c = [0.85, 0.90, 0.95, 1.00]$,
- variable deflection angle of the first rudder segment, $\delta_1 = [0, 10, 15, 20, 25 : 1 : 37]^o$,
- variable rudder *gearing ratio*, i.e. second rudder segment to first rudder segment deflection ratio $\delta_2/\delta_1 = [0.0 : 0.2 : 2.2]$.

3 Aerodynamic Analysis & Optimisation

The aerodynamic analysis comprises two subsequent phases. In the *aerodynamic optimisation* phase, multiple configurations with different choices of the rudder parameters x_{h2}/c, δ_1 and δ_2/δ_1 will be evaluated. The driving scenario corresponds to a one engine-out case (FAR25.149) at minimum control speed, V_{mc}. For a generic transport aircraft, representative tail onflow conditions are: $M = 0.15$, $\alpha = 5^o$, $\beta = -4^o$, $Re = 4.8 * 10^6/m$. The *optimisation constraint* is to ensure that the aircraft minimum control speed, V_{mc}, is not compromised when applying a reduced-size VTP with double-hinged rudder. This constraint translates into a requirement of constant maximum side force of the VTP with (fully-) deflected rudder. An aerodynamic force can be interpreted as the product of dynamic pressure, force coefficient and area. Hence, for constant VTP maximum side force at constant dynamic pressure, a VTP area reduction must be

accompanied by a VTP maximum side-force coefficient increment. As the *optimisation objective* is defined as minimum wetted VTP area, this translates directly into a search for VTP maximum side force coefficient at the given VTP onflow condition. The rudder deflection angle for VTP maximum side force coefficient is a another free variable in this optimisation process. Note that the rudder deflection angle at which VTP maximum side force coefficient occurs, is not necessarily identical for the different rudder candidates.

In summary, the optimisation procedure adopted is to select values for the rudder design parameters x_{h2}/c and δ_2/δ_1, to solve the VTP flow at fixed VTP onflow conditions for a rudder deflection sweep $\delta_1 = [0, 10, 15, 20, 25 : 1 : 37]^o$, and to extract the VTP maximum side force coefficient from this data set.

The aerodynamic optimisation procedure described above, results in a number of potentially interesting choices for the rudder design parameters x_{h2}/c and δ_2/δ_1. The geometry used in the aerodynamic optimisation studies is based on an isolated-VTP mounted on a symmetry plane. The symmetry plane effectively mirrors the flow solution at the VTP-root. In reality, the VTP is mounted on a fuselage/HTP which will only partly function as a mirror plane. Moreover, for high rudder deflection angles, a gap opens near the VTP-root promoting cross-flow between the rudder pressure and suction side. It is therefore to be expected that the isolated-VTP results will differ from the installed-VTP results. The final *aerodynamic assessment* of a number of selected configurations is therefore based on a fuselage/HTP installed-VTP geometry. These higher fidelity flow simulations will eventually determine the VTP size reduction potential that can be obtained with adopting an optimal double-hinged rudder solution.

3.1 Aerodynamic Optimisation Results

A block-structured Reynolds-Averaged Navier-Stokes flow solver (ENSOLV) is used to compute the flow around the candidate symmetry-plane mounted isolated-VTP configurations. Figure 1 illustrates the surface pressure coefficient distributions on the pressure & suction side of the VTP with single-hinged and a candidate double-hinged rudder VTP ($x_{h2}/c = 0.95$, $\delta_2/\delta_1 = 1.0$). The first rudder-segment deflection angle corresponds to the condition of maximum VTP/rudder side force coefficient values. The double-hinged solution shows a higher pressure differential over the rudder surfaces. Also, the VTP upstream of the first rudder segment hinge line shows a higher differential pressure. This is attributed to the induced circulation affecting the flow angles upstream of the configuration.

The VTP side force coefficients, as function of the first-rudder segment deflection angle, are extracted from the computations for each choice of the second rudder segment hinge line location x_{h2}/c and rudder gearing ratio δ_2/δ_1. Figure 2 presents the results. The maximum VTP side force coefficients occur at first rudder deflection angles in the range $25^o < \delta_1 < 35^o$. For the "fixed $x_{h2}/c = 0.85$ and variable δ_2/δ_1" double-hinged configurations, the maximum side force coefficient continues to grow with the rudder gearing ratio δ_2/δ_1 (Figure 2, left-hand side). For the "variable x_{h2}/c and fixed $\delta_2/\delta_1 = 1.0$" double-hinged configurations, the side force coefficients show a maximum at $x_{h2}/c = 0.95$ (Figure 2, right-hand side).

The maximum side force coefficient for the isolated-VTP with single-hinged rudder is $C_{Ymax} = 1.10$. Peak values of around $C_{Ymax} = 1.35$ are found for the isolated-VTP's with double-hinged rudders. Hence, the isolated-VTP double-hinged rudder concept offers an increase of around 23% in maximum side force coefficient capability. Two candidate solutions for the optimal double-hinged rudder parameters are identified:

- central hinge line location: $x_{h2}/c = 0.85$
  high rudder gearing ratio: $\delta_2/\delta_1 = 2.0$.
- aft hinge line location: $x_{h2}/c = 0.95$,
  unit rudder gearing ratio: $\delta_2/\delta_1 = 1.0$.

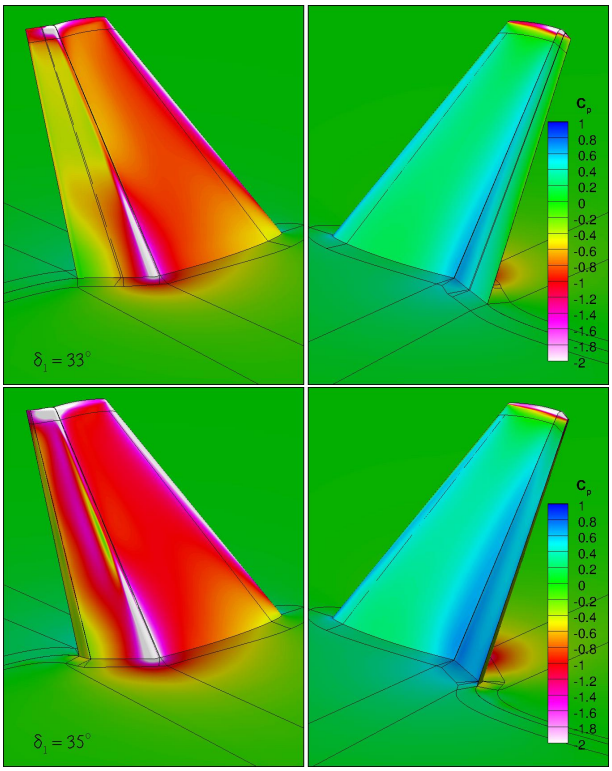

Fig. 1 Isolated-VTP surface pressure coefficient distribution for the single-hinged (top) and the $x_{h2}/c = 0.95$, $\delta_2/\delta_1 = 1.0$ double-hinged (bottom) rudder configurations.

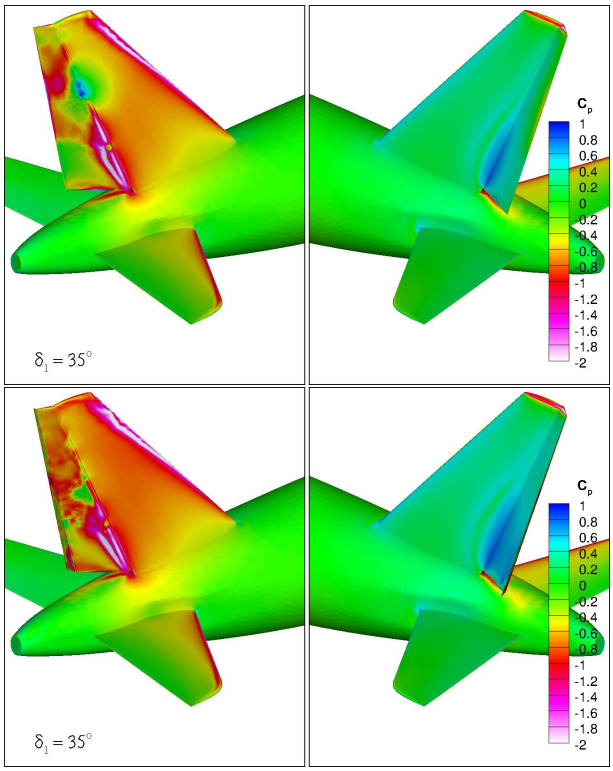

Fig. 3 Installed-VTP surface pressure coefficient distribution for the single-hinged (top) and the $x_{h2}/c = 0.95$, $\delta_2/\delta_1 = 1.0$ double-hinged (bottom) rudder configurations.

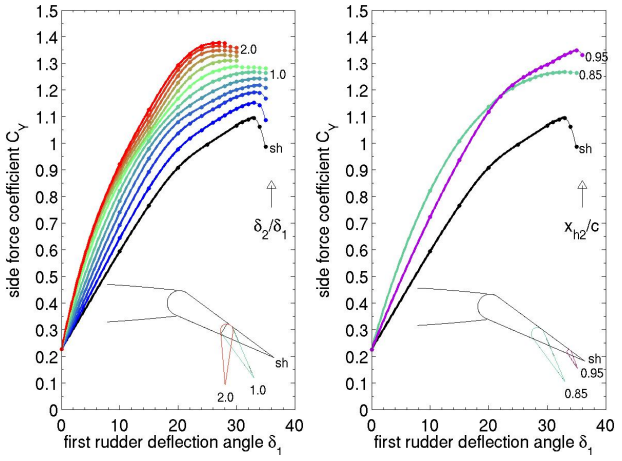

Fig. 2 Isolated-VTP side force coefficients for different rudder gearing ratios (left-hand side) and different second rudder segment hinge line locations (right-hand side).

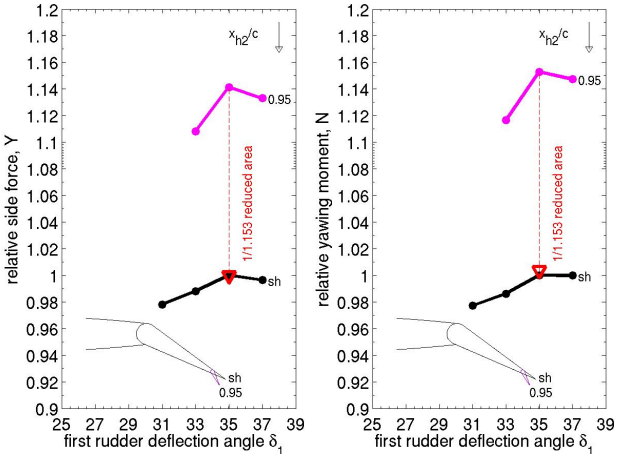

Fig. 4 Installed-VTP side force & yawing moment of the $x_{h2}/c = 0.95$, $\delta_2/\delta_1 = 1.0$ double-hinged rudder configuration relative to the single-hinged rudder results.

3.2 Aerodynamic Assessment Results

The reflection of the VTP flow in the symmetry plane may potentially lead to over-optimistic values for the VTP side force coefficients as found during the aerodynamic optimisation process. A final aerodynamic assessment of the selected candidate configurations is therefore conducted for a more complete geometry comprising a fuselage/HTP installed-VTP. Due to the increase in geometric complexity, an unstructured flow solver (TAU) is now used to provide flow solutions.

Figure 3 shows the installed-VTP pressure coefficient distribution for the single-hinged rudder versus one of the selected double-hinged rudder candidates: $x_{h2}/c = 0.95$, $\delta_2/\delta_1 = 1.0$. The first rudder deflection angle for maximum VTP side force coefficient is $\delta_1 = 35^o$. The pressure coefficient differential over the VTP & rudder is less pronounced compared to the results shown in Figure 1. The pressure differential decay at the VTP root due to "flow leakage" is apparent. On the other hand, the VTP pressure differential propagates on to the fuselage and HTP. Due to the high spanwise resolution of the computational mesh, the flow separations downstream of the cylindrical rudder leading edge are now well visible in terms of an irregular surface pressure distribution on the rudder suction side.

Figure 4 shows the (final 1000 iteration-averaged) complete configuration side force and yawing moment as function of the first rudder deflection angle for the single-hinged rudder and for one of the double-hinged rudder candidates: $x_{h2}/c = 0.95$, $\delta_2/\delta_1 = 1.0$. The force & moment data are scaled with the maximum values found for the single-hinged rudder configuration. Relative to the 23% force coefficient increment predicted for the isolated-VTP, the installed-VTP predictions are more conservative: 15.3% increment for the yawing moment coefficient.

A final verification is made for a 1/1.153 reduced-area VTP configuration, with double-hinged rudder parameters: $x_{h2}/c = 0.95$, $\delta_2/\delta_1 = 1.0$, mounted on the original-size fuselage & original-size HTP. The VTP is reduced around the root rear-spar location, $x_{spar}/c = 0.55$. The resulting side force and yawing moment for $\delta_1 = 35^o$, relative to the original-size VTP with single-hinged rudder, are given in Figure 4 by the red triangle symbols. It is concluded that this reduced-area VTP with $x_{h2}/c = 0.95$, $\delta_2/\delta_1 = 1.0$ double-hinged rudder indeed fully restores the original aircraft one engine-out minimum control speed performance.

3.3 Aircraft Cruise Drag Reduction

The impact of a 1/1.153 reduced-area VTP on total aircraft cruise drag is based on the following estimate,

$$\begin{aligned}\frac{(C_D)_{dh}}{(C_D)_{sh}} &= \frac{(C_D)_{w+f+htp} + (C_D)_{vtp} \cdot (\frac{S_{vtp}}{S_w})_{dh}}{(C_D)_{w+f+htp} + (C_D)_{vtp} \cdot (\frac{S_{vtp}}{S_w})_{sh}} \\ &= \frac{0.0265 + 0.0072 \cdot 0.175/1.153}{0.0265 + 0.0070 \cdot 0.175} \\ &= 0.9950\end{aligned}$$

hence, a 0.5% reduction in cruise drag. The drag coefficient of the VTP with double-hinged rudder is increased by 2.0 drag counts to account for a $h/c = 0.5\%$ additional second hinge rudder gap ($\Delta C_D = 1.3$ counts) and a lower Reynolds number ($\Delta C_D = 0.7$ counts). The VTP to wing area ratio is assumed to be 0.175 for the single-hinged rudder. Total aircraft drag in cruise corresponds to a lift over drag ratio of 18 at $C_L = 0.50$.

4 Rudder Actuation Systems

The aerodynamic optimization study (Section 3.1) resulted in two different double-hinged rudder concepts with identical performance. The second rudder segment drive mechanism is a non-trivial issue which impacts the final choice.

The actuation principle of the first rudder segment is identical for both the single-hinged and double-hinged solutions. It is assumed that the first rudder segment is driven by a linear hydraulic servo. A passive "push-bar" solution is selected to drive the second rudder segment. Figure 5 shows the actuation principle. The attachment point of this push-bar allows to control the

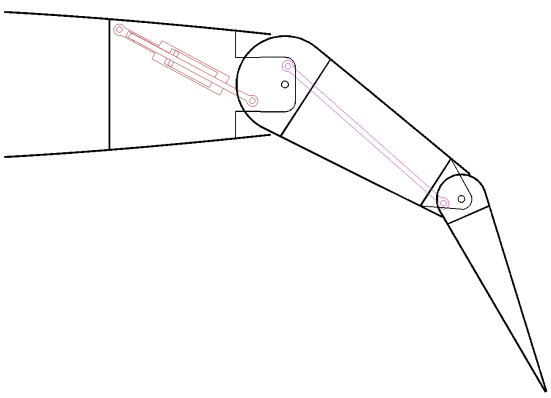

Fig. 5 VTP second rudder actuation principle by means of a push-bar solution.

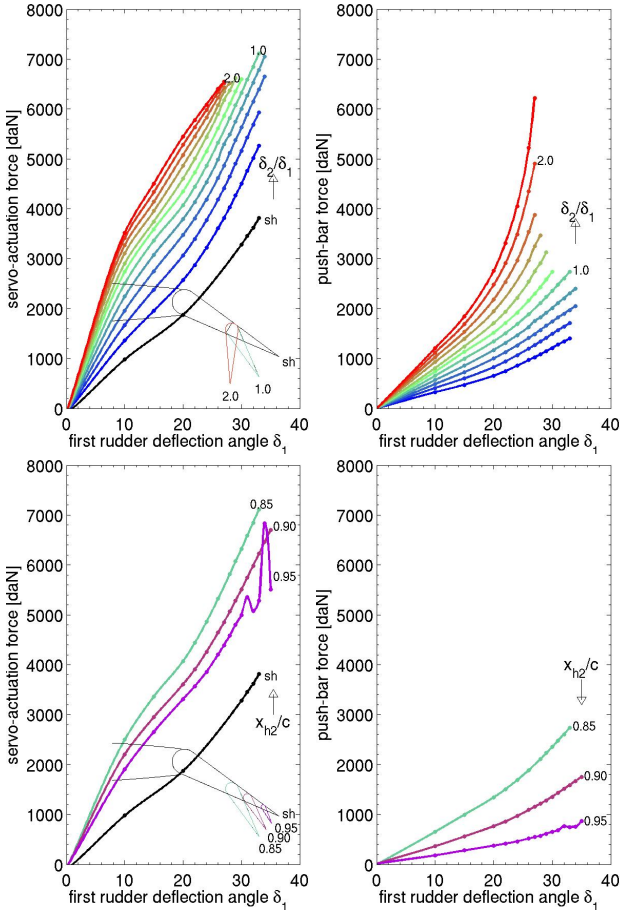

Fig. 6 Rudder servo forces (left-hand side) & push-bar forces (right-hand side) for different rudder gearing ratios (top) and different second rudder hinge line locations (bottom).

deflection rate of the second rudder segment relative to that of the first rudder segment. For a relatively far aft location of the second rudder segment hinge line, an internal push bar solution may lead to very small effective hinge moment arms of the push bar. In such cases, an external solution may be found.

Figure 6 shows that the servo forces and push-bar forces for maximum rudder deflections are a strong function of the double-hinged rudder design parameters x_{h2}/c and δ_2/δ_1. The trends are opposite, however. Increasing the rudder gearing ratio leads to higher VTP maximum side force capabilities at the cost of higher servo and push-bar forces. Locating the second rudder segment hinge line further aft also leads to higher VTP maximum side force capabilities but now the required servo and push-bar forces decrease.

It is therefore concluded that a relatively far aft location of the second rudder segment hinge line, $x_{h2}/c = 0.95$, provides an interesting increase in VTP maximum side force capability at a relative low increment of the servo actuation force and push-bar force. For this particular solution, an external push-bar solution may be required.

5 Flight Mechanics & Simulation

The stability and control analysis evaluates a number of critical manoeuvres required for compliance with the design and certification requirements (FAR/JAR25 and MIL-STD-1797A). The objective is to assure that lateral-directional handling quality levels are not degraded for the aircraft with the reduced-size VTP & double-hinged rudder relative to the aircraft with original VTP & single-hinged rudder.

To this end, a full non-linear aircraft simulation is used with adapted values for the aerodynamic derivatives to account for a 20% reduced VTP surface area:

$$C_{Y\beta dh} = 0.86 \cdot C_{Y\beta sh} \quad , \quad C_{Yrdh} = 0.87 \cdot C_{Yrsh}$$
$$C_{n\beta dh} = 0.70 \cdot C_{n\beta sh} \quad , \quad C_{nrdh} = 0.88 \cdot C_{nrsh}$$

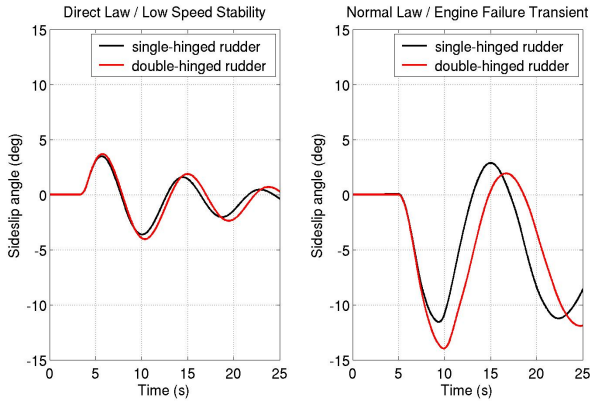

Fig. 7 Sideslip excursions following a 1 second full rudder deflection (left-hand side) and an engine failure (right-hand side).

Figure 7, left-hand side, shows the low-speed aircraft sideslip response following a 1 second full rudder deflection. No yaw damper functionality is active in this simulation. Some effect of the reduced-size VTP on Dutch roll eigenfrequency and damping is noticeable. However, this level of basic-airframe lateral stability degradation is not found to be significant.

Figure 7, right-hand side, shows the overswing sideslip angles that occur after engine failure at $1.1 \cdot V_{mc}$. A 20% increase in peak sideslip angle is observed for the aircraft with reduced-size VTP. This holds a risk of VTP stall. Note that in this case the yaw damper is active. The yaw damper feedback gains were identical and not adapted in case of the reduced-size VTP. Preventing VTP stall under these circumstances may call for higher yaw damper gains or, alternatively, a larger nose radius of the VTP airfoils to delay VTP stall angles.

None of the handling qualities studies that were performed (Figure 7 illustrates only two examples, more cases were actually studied) revealed a potential show stopper for a VTP surface area reduction up to 20%.

6 Tail Loads

FAR25.351 presents an overswing sideslip manoeuvre as one of the limit load conditions for the VTP. This manoeuvre comprises three individual parts:

· Case 1: pilot commands full rudder until the rudder stop.

· Case 2: with the rudder stop, the aircraft reaches maximum (overswing) sideslip angle.

· Case 3: after reaching steady sideslip conditions, rudder is returned to neutral position.

A single flight condition has been selected (dive @ M=0.90 & h=24,600 ft) with the single-hinged rudder travel limiter set equal to $\delta_{max} = 3.4^o$. For the corresponding double-hinged rudder case, the rudder travel limiter has been adjusted to arrive at identical steady state sideslip performance capabilities of the aircraft: $\delta_{1max} = 2.7^o$.

The flight simulation setup (Section 5) with adapted values for the aerodynamic derivatives, has been used to evaluate the tail loads manoeuvre. CFD is applied to the isolated-VTP setup described in Section 3.1 to compute the corresponding surface pressure loading.

7 Structural Mechanics

The double-hinged rudder device is expected to come at a mass penalty. However, this mass penalty may well be compensated by the overall VTP size reduction. A structural analysis & design tool is described and subsequently applied to the candidate VTP's to quantify the impact of the double-hinged rudder on overall aircraft mass.

7.1 Structural Analysis & Design Tool

A two-level structural analysis & design system is used, Figure 8. At the top-level it performs Finite Element Method (FEM) calculations, sizing the (composite) structure in a stress driven design. At the second-level, analytical models are used to translate structural detail design considerations into allowable stress levels to be incorporated at the top-level.

The overswing sideslip manoeuvre (Section 6) is used to derive three mechanical load cases driving the top-level structural sizing. For this purpose, the aerodynamic surface pressure are

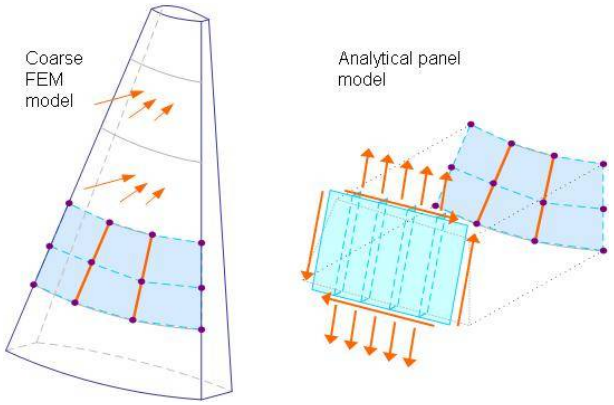

Fig. 8 Two-level structural analysis & design method.

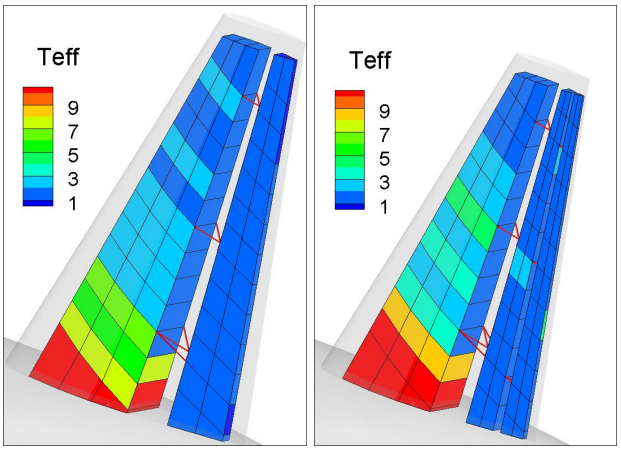

Fig. 9 Effective material thickness distribution for the full-size VTP & single-hinged rudder (left-hand side) versus the 20% reduced-area VTP & double-hinged rudder (right-hand side).

mapped to structural grid force vectors using surface spline interpolation techniques. The structural sizing is driven by the MSC Nastran SOL200 optimiser. The FEM model comprises shells and beams representing the primary VTP structure: covers, spars, ribs and schematically the hinges and actuators. Stiffeners are represented as lumped beams. The shell (ply-) thicknesses are used as design variables resulting in optimal thicknesses given the applied loads. Besides applied loads, allowable stress levels are required in order to complete this stress driven optimisation.

The attainable stress levels result from a second-level optimisation, which is based on analytical models and/or detailed skill tool analyses. These detailed analyses include considerations like rib crushing, panel buckling (flexural, local and shear), maximum strains and servo system forces. At this second level, a stiffened panel is used to represent an appropriate surface area within the FEM model. Applied panel loads are deduced from the momentary FE-stress levels. Stringer geometry, thickness and skin thickness are used as local design variables to find a feasible design with minimal weight. The resulting analytical design is translated at FEM-level into new shell thicknesses and lumped stringer properties. The achieved panel stress levels are translated towards stress constraint allowables within the global FEM-optimisation (top-level).

7.2 VTP Mass Estimates

Two VTP candidates were analysed: the full-scale single-hinged rudder VTP, serving as a reference, and a 20% reduced area ($x_{h2}/c = 0.85$, $\delta_2/\delta_1 = 1.0$) double-hinged rudder VTP. Figure 9 shows the effective skin thickness distribution of the two configurations. Interpolation linearly to the 1/1.153 area reduction of the selected ($x_{h2}/c = 0.95$, $\delta_2/\delta_1 = 1.0$) double-hinged rudder candidate, results in a negligable VTP mass change relative to the full-scale single-hinged rudder VTP. This result combines a 40% increase of secondary mass (hinges & actuators) and a 8% decrease of primary mass (VTP structural box & rudders). In theory, the decrease of primary mass is almost proportional to the area reduction, in case only constant gauge limits apply. The achieved VTP primary mass reduction, relative to the full-scale double-hinged rudder, lies near this value. Detailed evaluation of the structural optimisation results revealed that for the "outer" parts of the VTP the applied loading was indeed non-sizing and thicknesses ran towards minimum gauge.

The effect of additional load cases (e.g. turbulence loads) has not been evaluated. A similar analysis for a double-hinged HTP design (conducted by Airbus-Spain) revealed a flutter insta-

bility for high aspect-ratio second elevator segments. Stiffness related properties, therefore, are expected to be important drivers as well.

8 Conclusions

The aerodynamic optimisation study delivered two potentially interesting double-hinged rudder concepts:

$$x_{h2}/c = 0.85 \quad , \quad \delta_2/\delta_1 = 2.0$$
$$x_{h2}/c = 0.95 \quad , \quad \delta_2/\delta_1 = 1.0$$

which showed 23% increase in isolated-VTP maximum side force coefficient potential. The higher fidelity installed-VTP computations resulted in a more conservative estimate of 15.3% maximum yawing moment coefficient increment for the $x_{h2}/c = 0.95$, $\delta_2/\delta_1 = 1.0$ double-hinged rudder case relative to the single-hinged rudder baseline.

For a generic medium-range transport aircraft, the cruise drag saving is estimated to be 0.5% when employing this double-hinged rudder concept.

A second rudder drive mechanism, by means of a mechanical "push-bar", was proposed. The servo force increments and push-bar forces were analysed. This led to a preference for the second double-hinged rudder candidate.

The effect of a reduced size-VTP on the aircraft lateral/longitudinal handling qualities was investigated. Damping of the Dutch roll eigenmotion is somewhat degraded. Transport aircraft generally require artificial stabilisation devices anyway (yaw dampers) and this effect is not believed to present a show stopper. Engine failure transients result in higher overswing sideslip angles for the reduced-size VTP case. This holds a risk of VTP stall. This may call for higher yaw damper gains or, alternatively, a modification to the VTP nose section shape to delay stall.

VTP loads were assessed and a VTP mass estimate was performed. Although the double-hinged VTP in principle comes at the cost of an increase in mass, the VTP area reduction reduces this mass again. It is believed that the nett effect is an almost constant VTP mass.

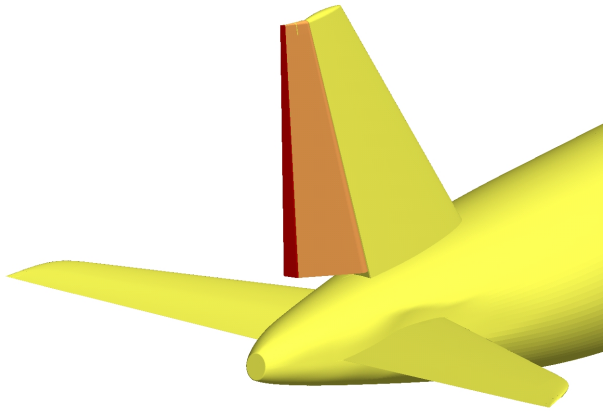

Fig. 10 Proposed optimum double-hinged configuration featuring a relatively small second rudder segment.

Figure 10 shows an impression of the proposed VTP with double-hinged rudder.

9 Acknowledgements

This research is 50% funded by the European Commission in the 6-th framework programme *New Aircraft Configuration REsearch* (NACRE) and 50% by NLR's programmatic funding, Theme 12: Future Technologies for High Tech Systems. The technical work reported in this paper is carried out close collaboration with partners in the NACRE project.